Supporting Information

EMM-23: a stable high silica multi-dimensional zeolite with extra-large tri-lobe shaped channels

Tom Willhammar[†,§], Allen W. Burton[‡,§,*], Yifeng Yun[†], Junliang Sun[†], Mobae Afeworki[‡], Karl G. Strohmaier[‡], Hilda Vroman[‡], Xiaodong Zou[†,*]

[†] Inorganic and Structural Chemistry and Berzelii Center EXSELENT on Porous Materials, Department of Materials and Environmental Chemistry, Stockholm University, Stockholm SE–106 91, Sweden

[‡] Corporate Strategic Research, ExxonMobil Research & Engineering Co. Inc, 1545 Route 22 East, Annandale, New Jersey 08801, USA.

[§] These authors contributed equally.

Materials and methods

1. Synthesis

The synthesis of the OSDA is described in Reference 1. The syntheses are performed by adding 10.0 mmol Si from tetramethylorthosilicate (TMOS, 1.54 g) to 5.0 mmol of OH^- from an aqueous solution of the diquat that has been ion-exchanged into its hydroxide form. If alumina (alumina trihydrate, Alcoa-C31) is used in the synthesis, it is mixed with the hydroxide source *prior* to the addition of the TMOS. After all of the ingredients have been added, the Teflon liners are placed within a vented hood to allow the methanol and water to evaporate. Unlike syntheses which use large F/Si ratios (~0.5), the gels are not thick, white pastes; instead they are transparent gels with a gummy or sappy consistency. After sufficient time has been allowed for the evaporation, sufficient water is then added back to the liners to bring the H_2O/Si to 5. The Teflon liner is capped and sealed inside a steel Parr autoclave. All of the reactions are carried out at 150 °C in 23-mL tumbling (~ 50 rpm) autoclaves. After 10 days of heating, the autoclaves are removed from the ovens and quenched to ambient temperature. The suspensions are then vigorously mixed to homogenize the suspension and a small portion of the sample is removed with a spatula. The small sample portion is then filtered, washed with deionized water, and dried. After drying, PXRD is collected on each sample to check the crystallinity.

2. Characterization

Electron microscopy:

The as-made sample was used for the TEM study, since it has the highest crystallinity. The sample was crushed in an agate mortar, dispersed in ethanol and finally applied to a holey carbon grid.

High resolution transmission electron microscopy (HRTEM) images were acquired on a JEOL JEM 2100F microscope operated at 200 kV with a Gatan Ultrascan 1000 camera. Each of the structure projection images were reconstructed from a through-focus series of 20 HRTEM images acquired with a constant focus step of 103 Å. The processing was done using the software QFocus[2]. Plane group determination from the structure projection image was done using the software CRISP[3].

Rotation Electron Diffraction (RED) data was collected using a JEOL JEM 2100 microscope operated at 200kV using a single tilt tomography holder. The electron diffraction frames were acquired by an upper mounted Gatan ES500W Erlangshen camera. The RED data was collected and processed using the software package RED[4-5]. 352 electron diffraction frames were collected covering a tilt range from -70.82° to - 7.08° with a tilt step of 0.2°.

The structure of EMM-23 was solved using the RED data based on the space group *P*-62*c*. The structure determination of EMM-23 from RED intensities was performed by direct methods using the program SHELX[6].

Solid-state NMR:

CPMAS (cross-polarization, magic-angle spinning) ^{13}C and Bloch decay (BD) MAS ^{29}Si NMR spectra were recorded using a Varian InfinityPlus 500 spectrometer operating at 11.7 and 9.4 T, corresponding to Larmor frequencies of 125.5 (^{13}C), and 99.2 and 79.3 (^{29}Si) MHz, respectively. The ^{13}C CPMAS spectrum was obtained using a 5mm probe head at MAS rate of 8 kHz, using a contact time of 0.3 ms, a decoupling pulse of 62.5kHz, and a recycle delay of 10 s. Quantitative ^{29}Si MAS NMR spectrum was obtained using a 7.5 mm probe head at MAS rate of 5kHz, a decoupling pulse of 62.5 kHz and a pulse delay of 180 s. 79.3 MHz ^{29}Si MAS NMR spectrum of the calcined sample was obtained using a 7.5 mm probe head at MAS rate of 5kHz, a decoupling pulse of 62.5 kHz and a pulse delay of 60 s. The chemical shifts shown are with respect to tetramethyl silane at 0 ppm for both nuclei.

Rietveld refinement of the as-made form of EMM-23:

Synchrotron data were collected at Brookhaven National Labs X-10B beamline with a wavelength of 0.8668 Å. The samples were placed in a 1 mm quartz capillary (Debye-Scherrer geometry). The polarization factor was 0.93 with monochrometer and 0.50 without monochrometer. The data was normalized by adjusting the counting time (9-16 s) for a step to a reference monitor beam to account for variation in the beam intensity during the measurement. Rietveld refinement of the as-made material was carried out using the program GSAS[7] and the refinement of the ozone treated material was done using TOPAS[8].

Due to the extra-large pores and the presence of disordered Q^2 and Q^3 species, it has been very challenging to locate the OSDAs directly. For the starting model, we used an energy-optimized configuration of the OSDA molecule using the Cerius2 software with the Universal-Burchart forcefield.[9-10] within the pores that matches the 3-fold symmetry of the framework. The propyl groups at each end of the OSDA point within the cages bound by 10-ring windows. This molecule was placed in the model with ½ occupancy (3 molecules/ per unit cell). However, the refinement of the organic molecule was not well-behaved and the bond geometries of the framework were not ideal. The refinement pushed the organic molecules toward the framework so that the ends of the propyl groups were prohibitively close or overlapping within the cage at the intersection of the 10-ring pores. This suggested that there was missing electron density within the centers of these cages. When we placed water molecules within the cages, we still could not rectify the geometric problems of the model. We then considered another configuration in which one end of the OSDA molecule was contained within the cage with the nitrogen near the center, the pyrrolidine ring positioned near one 10-ring, the propyl pointing to another 10-ring, and the methylene chain passing through the last 10-ring so that the other end of the OSDA molecule was positioned within one of the lobes of the trilobe. The optimized energy indicated that this configuration was more energetically stable than the first one. However, since there are only two cages per unit cell, only two molecules can be in this configuration within each unit cell. One additional molecule can be placed in the third lobe with its methylene chain approximately parallel to the 3-fold symmetry axis rather than approximately perpendicular as found for the molecules of the first configuration. In this arrangement

(Figure 3d), there is less empty space near the center of the pores when compared to the previous model with the three symmetry-equivalent molecules. When incorporated into the model, the fractional occupancies of the molecules in these configurations refined to the expected values of 0.333 and 0.167, respectively, and the bond geometries of the zeolite were more chemically acceptable than those in the initial model with a single type of configuration for the OSDA molecule. However, there were still problems with the bond geometries of the silicon sites located within the cusps of the trilobes at the expected positions of the Q^2 or Q^3 species. At this point, water was located at three different positions close to the oxygen atoms. After these water sites were incorporated into the model, the bond geometries of the sites within the cusps became more ideal. The total water content refined to about 4 water molecules/per unit cell (about 1 wt%). There are two different silicon sites (Si4 and Si11) that occupy the cusps between the lobes. The refined occupancies of these sites are 0.33 and 0.67, respectively – almost exactly 1/3 and 2/3. The final agreement factors were Rwp=10.2%, Rp=7.61% and $\chi^2 = 2.41$.

Because Si4 and Si11 are next nearest silicon neighbors, a Q^2 site is created when only one of the sites is absent. The occupancies of these sites are correlated with the configurations of the OSDA molecules in the lobes which surround each cusp. Si11 and Si4 occupy 2/3 and 1/3, of these cusp sites, respectively (See Figure S9). If either Si4 or Si11 is always absent within a given column of cusp sites along the ***c***-axis, then the Q^3:Q^2 ratio will be 2 within that column. However, it is likely that the arrangement is random along the ***c***-direction because the configurations of the OSDA may vary within each lobe along the ***c***-direction. Interestingly, the position of Si4 along the ***c***-axis is similar to that of the nitrogen atom in configuration 1; *i.e.*, its position is closer to the positive charge of OSDA1. Conversely, the position of Si11 along the ***c***-axis is similar to that of the nitrogen atom in configuration 2. The minimized distances between the positively charged N atom and the O atoms of the Q^2 explain the correlation between the occupancies of the OSDA cations and those of Si4 and Si11. The O atom between Si4 and Si11 is split between two different positions (O9' and O9") which have fractional occupancies of 1/3 and 2/3, respectively. The position of this oxygen atom is expected to vary according to which silicon sites are occupied. Likewise, atoms O20 (1/3 occupancy) and O19 (2/3 occupancy) are connected only to atoms Si4 and Si11, respectively.

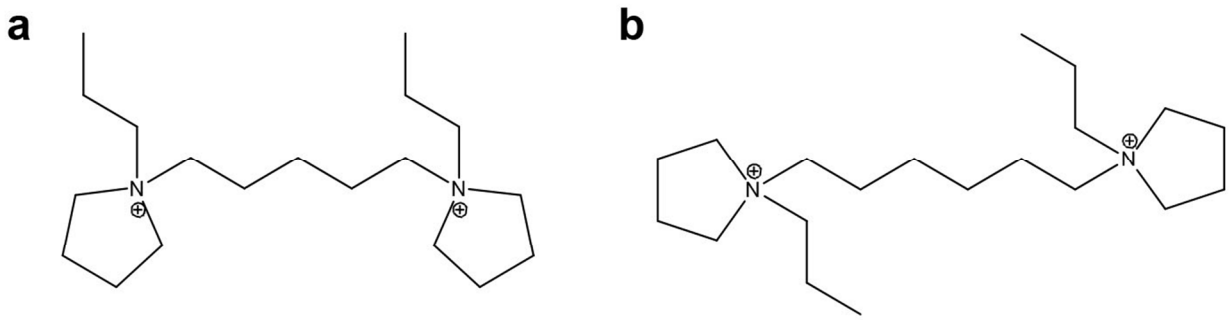

Figure S1. The two organic structure directing agents (OSDAs) used to prepare EMM-23. (a) 1,1-(pentane-1,5-diyl)bis(1-propylpyrrolidinium) hydroxide and (b) 1,1-(hexane-1,6-diyl)bis(1-propylpyrrolidinium) hydroxide.

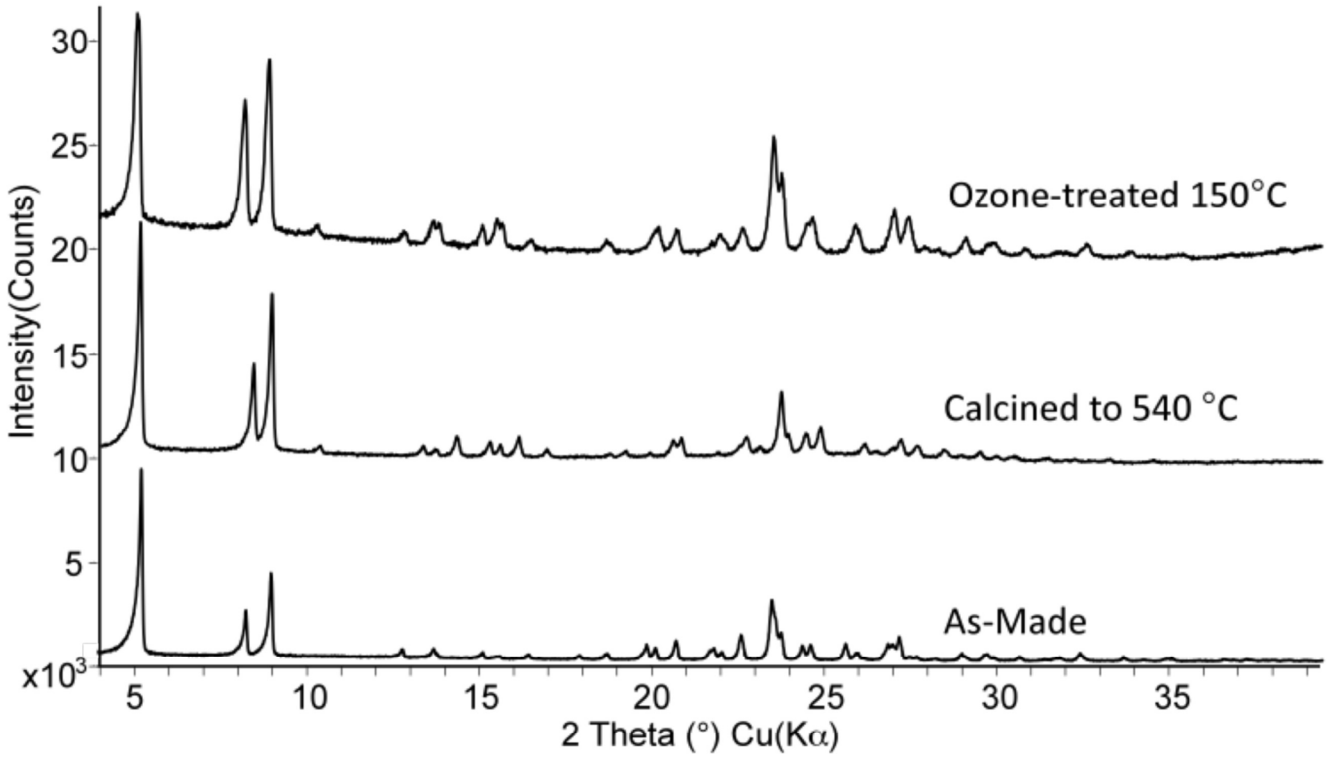

Figure S2. Powder XRD Patterns of as-made (bottom), calcined (middle) and ozone-treated (top) EMM-23.

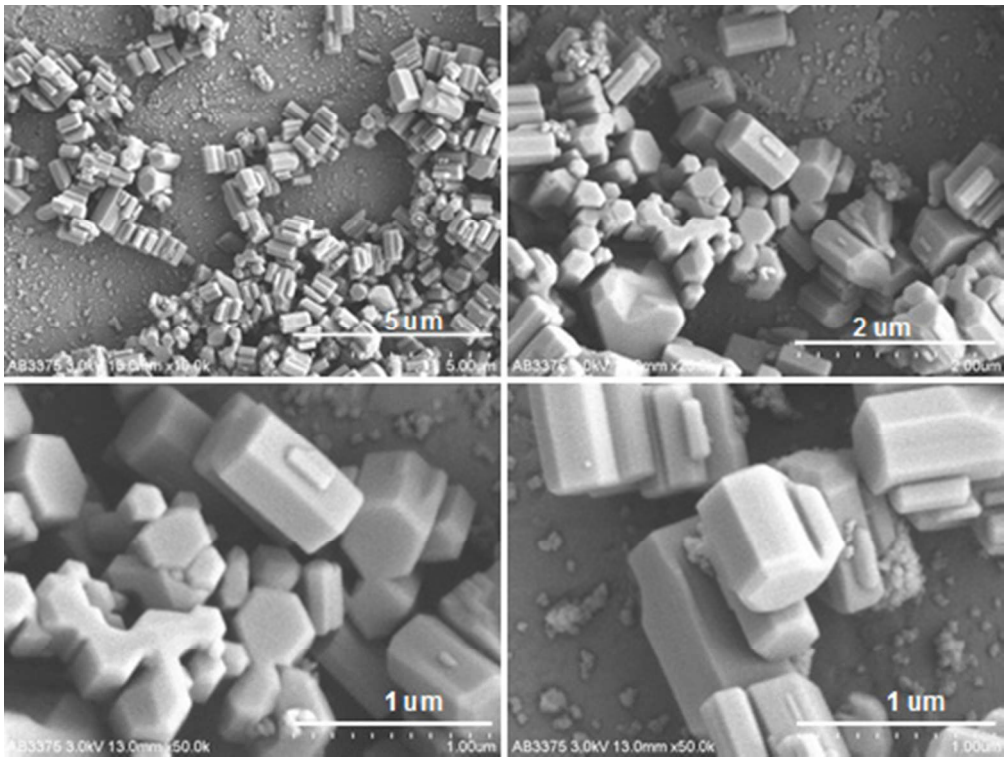

Figure S3. SEM images of EMM-23 at different magnifications. The point group symmetry of the structure is reflected in the morphology of the crystals.

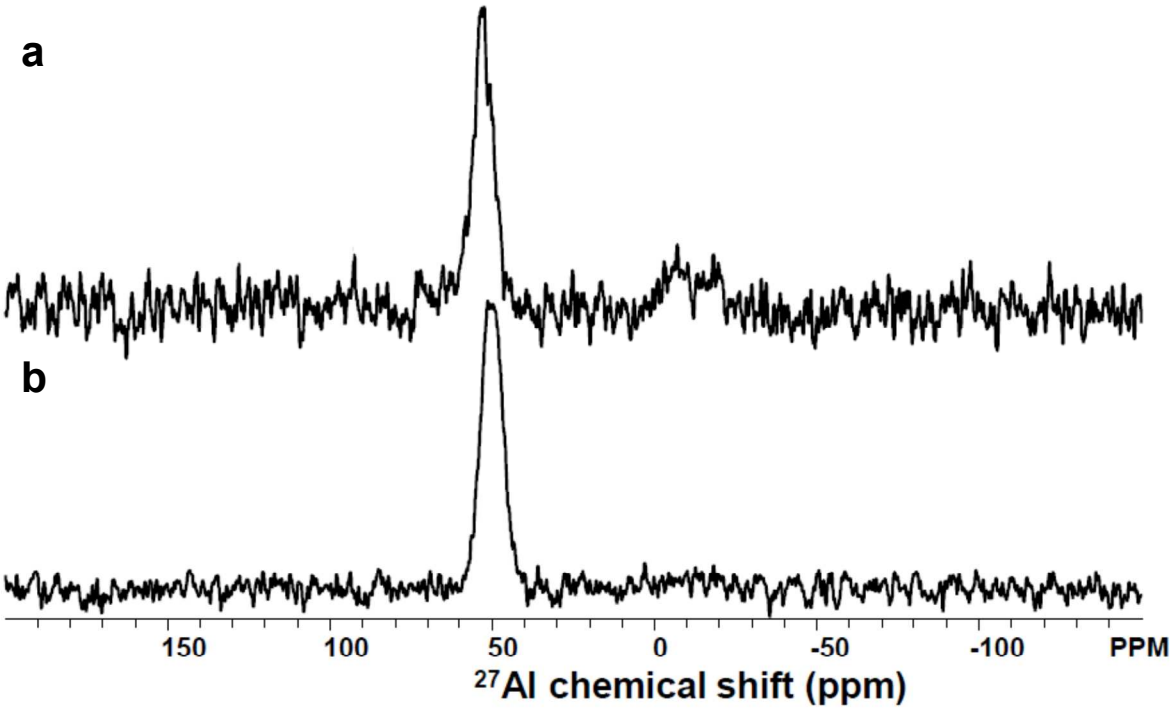

Figure S4. ^{27}Al MAS NMR spectra of (a) as-made EMM-23 and (b) calcined EMM-23 with Si/Al ratio of 50.

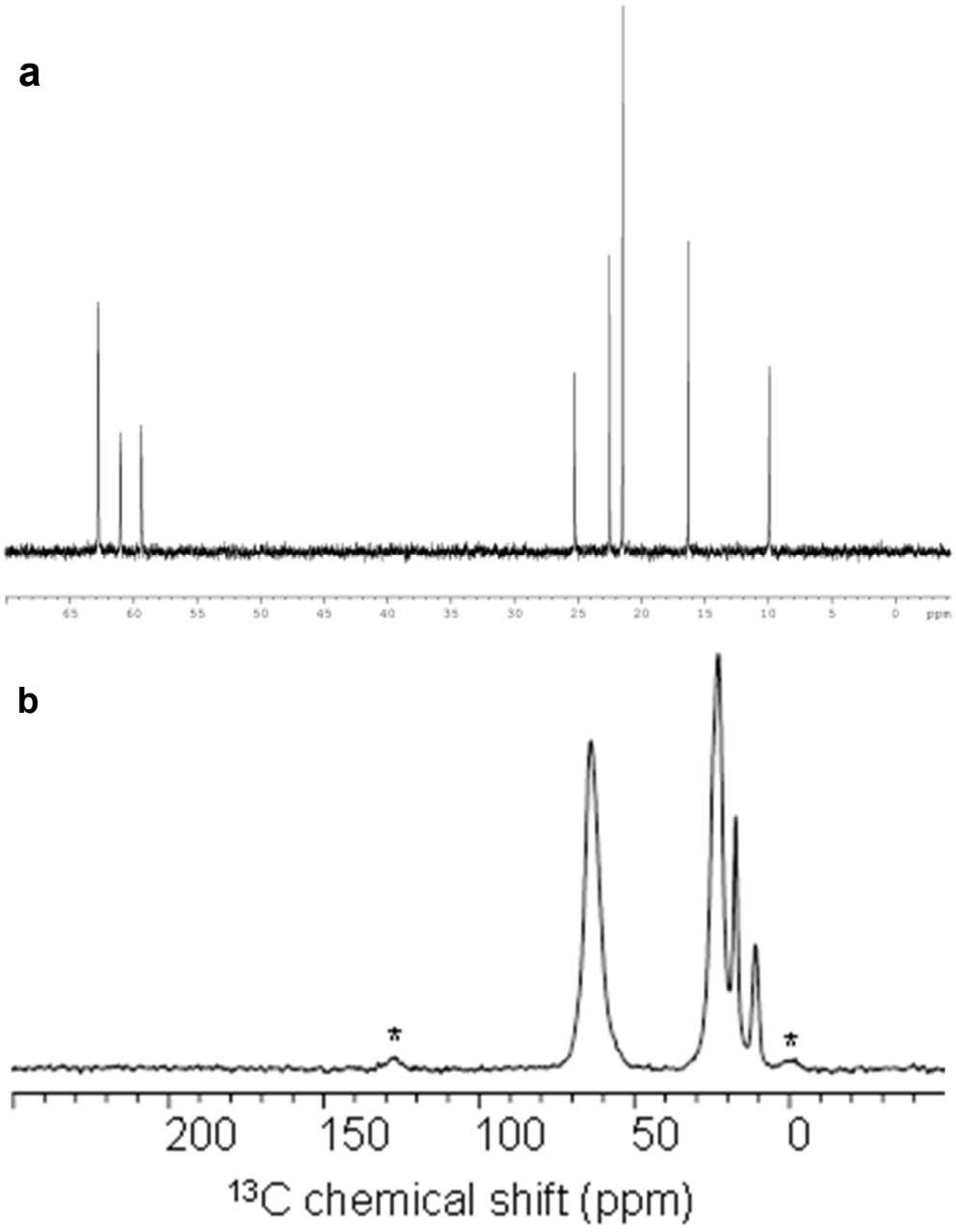

Figure S5. (a) ^{13}C NMR spectrum of 1,1-(pentane-1,5-diyl)bis(1-propylpyrrolidinium) hydroxide shown in Figure S1a and (b) cross-polarization, magic-angle spinning (CPMAS) ^{13}C NMR spectrum of EMM-23, prepared with 1,1-(pentane-1,5-diyl)bis(1-propylpyrrolidinium) hydroxide, acquired at 11.7 T. Asterisks represent spinning sidebands.

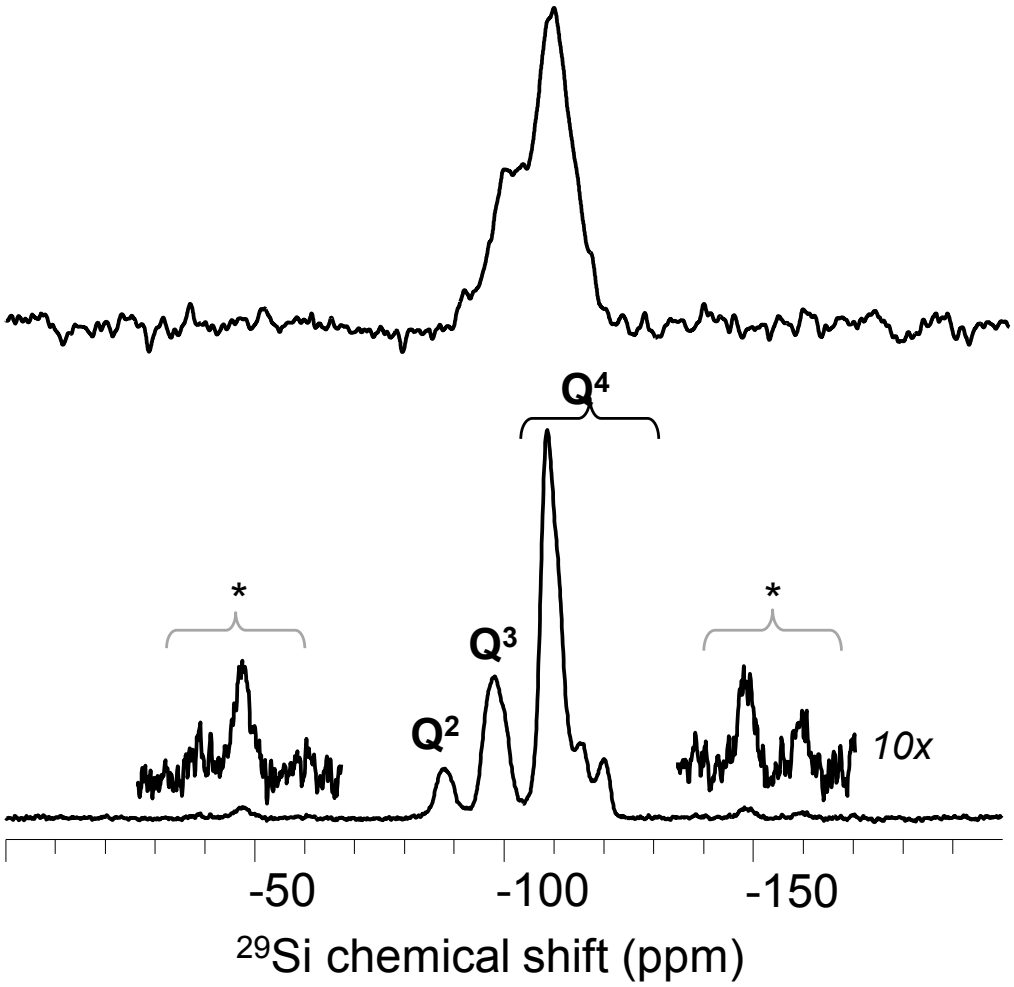

Figure S6. ^{29}Si MAS NMR spectrum of calcined (top, 79.3MHz) and as-made (bottom, 99.2 MHz) EMM-23, showing Q^2, Q^3, and Q^4, asterisks denote spinning sidebands.

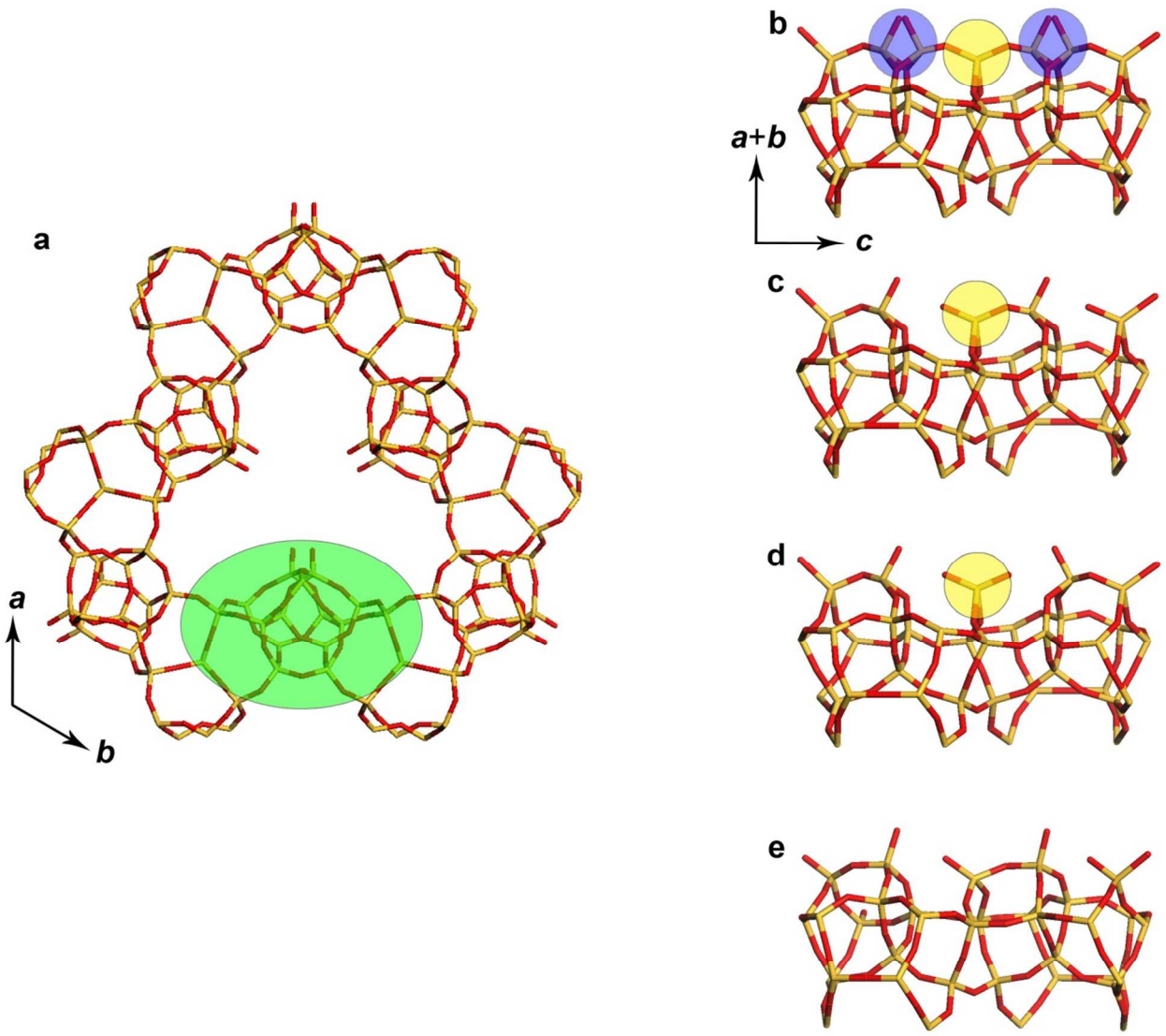

Figure S7. Evaluation of coordination in the framework of EMM-23. (a) The structure model of EMM-23 viewed along [001] with the "cusps" sites marked by a green oval. (b-d) The region around the "cusps" sites of the structure model in space group *P*-62*c* viewed along [1-10]. The sites marked by a blue circle are partially occupied, which results in the yellow atom being either (b) Q^4, (c) Q^3 or (d) Q^2 depending upon which of the symmetry-equivalent tetrahedral atoms are removed. (e) The region around the "cusps" sites of the structure model in space group *P*31*c* viewed along [1-10].

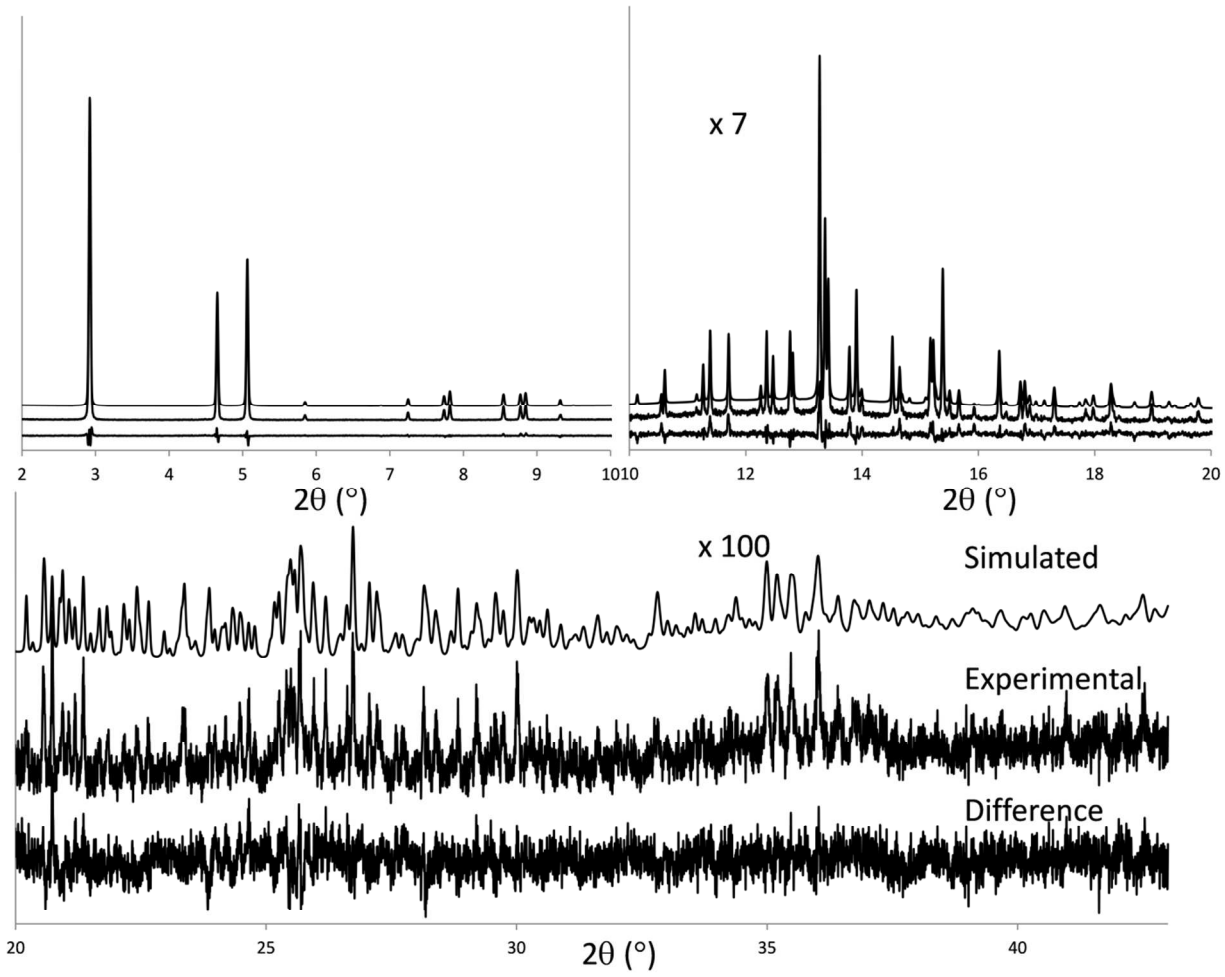

Figure S8. Calculated (top traces), experimental (middle traces) and difference (bottom traces) PXRD profiles for the Rietveld refinement (λ=0.8668 Å) of the ozone-treated EMM-23. The agreement R-values are Rp = 8.35%, Rwp = 11.1%, and Rexp = 8.13%.

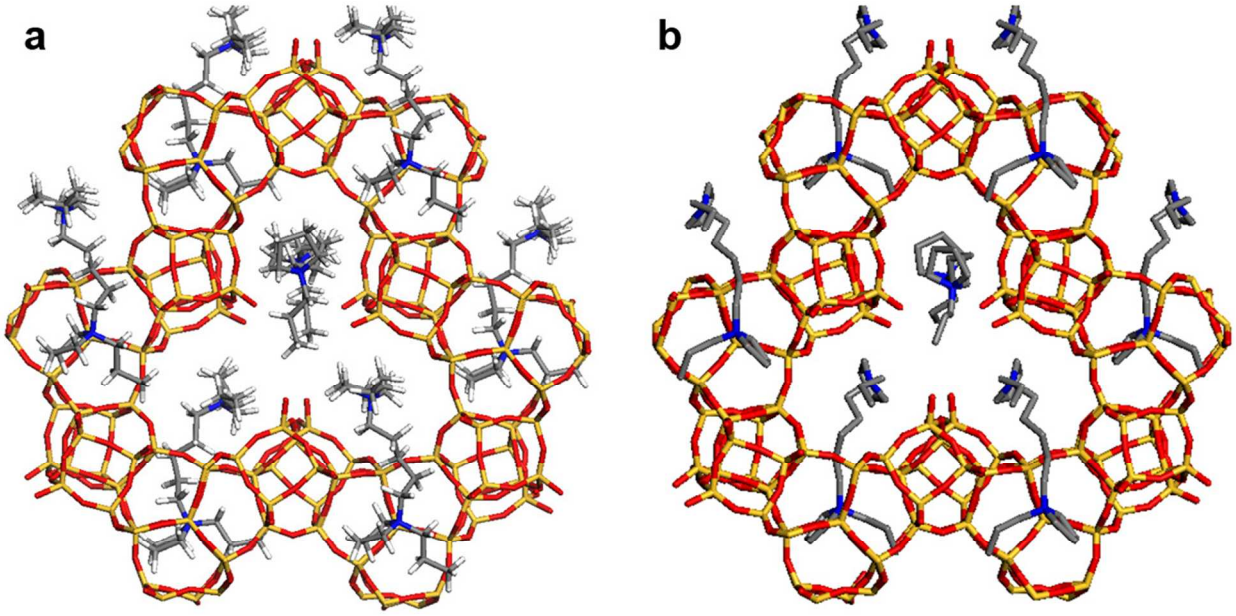

Figure S9. Location of OSDA in EMM-23. (a) Energy-optimized configuration of OSDA molecules with two symmetry-independent positions for the OSDA molecules. (b) The model showing the two different OSDA configurations after Rietveld refinement. The OSDA molecules in the bottom lobes in (b) are related by symmetry. The silicon atoms are yellow, the oxygen atoms are red, the carbon atoms are grey, the nitrogen atoms are blue, and the hydrogen atoms are white.

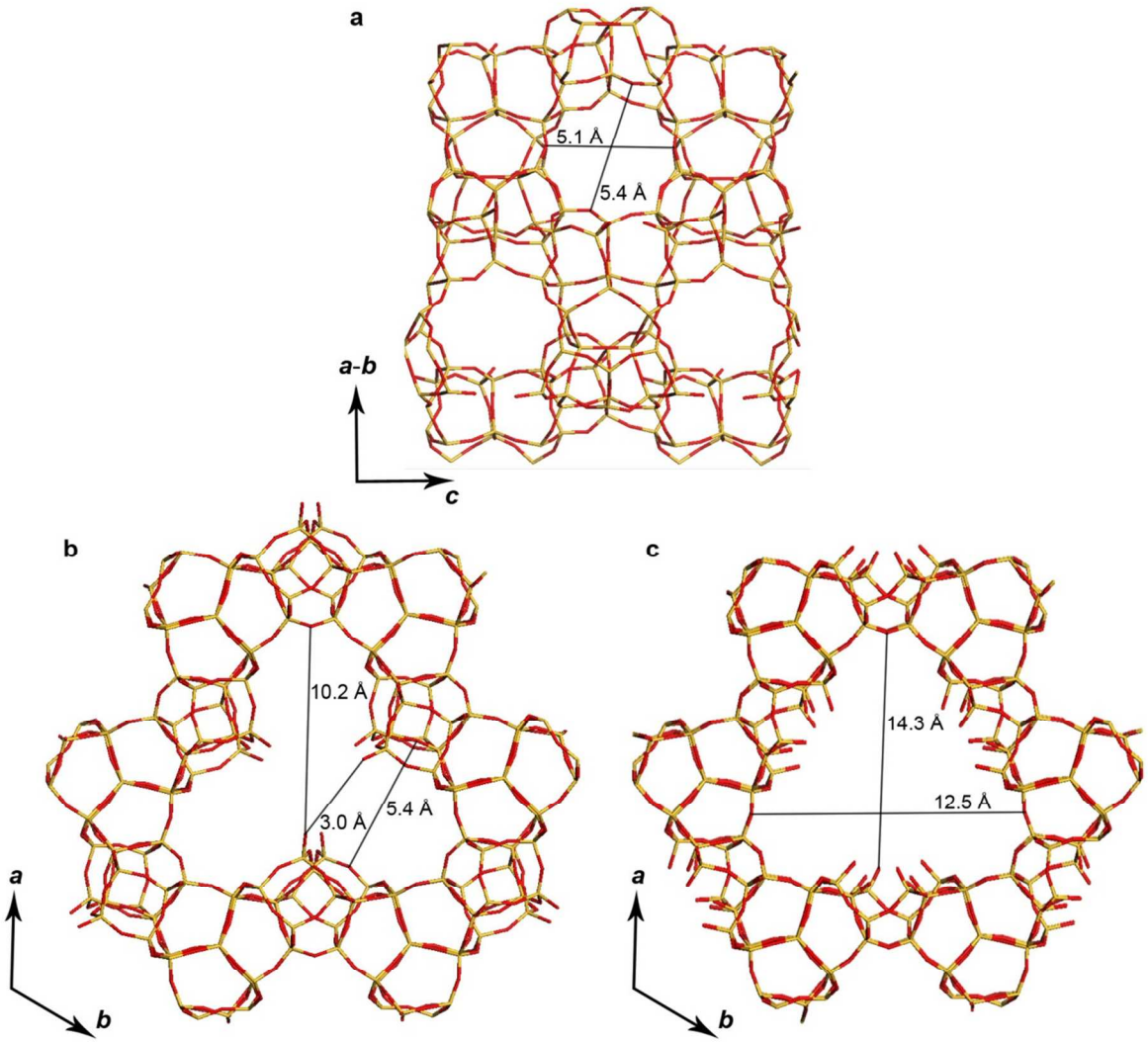

Figure S10. Pore sizes in EMM-23. The free diameters for the channel windows of EMM-23 for the (a), 10-ring channels viewed along the ***a***+***b***-axis, (b) 21-ring channel along the ***c***-axis for the structure model with all T-atoms occupied and (c) 24-ring along the ***c***-axis for the structure model with the partially occupied T-atoms absent. The marked distances are after subtracting two van der Waals radii for oxygen, 2.7 Å.

Table S1. Crystal data and refinement results. 3D-RED data collection, crystal data and structure refinement details of EMM-23.

Tilt range	-70.82° to -7.08°
Tilt step	0.20°
No. of ED frames	352
Exposure time/ s/frame	4.0
a / Å	20.00
b / Å	19.92
c / Å	13.38
α / °	91.73
β / °	89.60
γ / °	120.23
Completeness	89.1% (resolution cut to 1.15 Å)
R_{int}	0.4147
No. of measured reflections	3895
No. of unique reflections	1021
h	$-15 \leq h \leq 15$
k	$-13 \leq k \leq 13$
l	$-13 \leq l \leq 13$
*R*1	0.3577
No. of parameters	78

Captions for the movies S1-S2

Movie S1. A movie displaying the 352 original ED frames covering a tilt range from -70.82° to -7.08° with a tilt step of 0.2° collected by the RED method.

Movie S2. A movie showing the three-dimensional reciprocal lattice of EMM-23 reconstructed from the RED data, which was used for ab initio structure solution of EMM-23 by direct methods.

Movie S3. A movie showing the three-dimensional atomic structure of EMM-23.

Captions for attached Crystallographic Information Files

EMM23_as-made.cif Crystallographic Information File containing the atomic coordinates after Rietveld refinement of the as-made treated EMM-23.

EMM23_ozone.cif Crystallographic Information File containing the atomic coordinates after Rietveld refinement of the ozone treated EMM-23.

References

1. Burton, A. W.; Strohmaier, K. G.; Vroman, H. Patent Application WO201319462 **2013**.
2. Wan, W.; Hovmöller, S.; Zou, X.D. *Ultramicroscopy* **2012**, *115*, 50.
3. Hovmöller, S. *Ultramicroscopy* **1992**, *41*, 121.
4. Wan, W.; Sun, J.L.; Su, J.; Hovmöller, S.; Zou, X.D. *J. Appl. Cryst.* **2013**, *46*, 1863.
5. Zhang, D.L.; Oleynikov, P.; Hovmöller, S.; Zou X.D. *Z. Kristallogr.* **2010**, *225*, 94.
6. Sheldrick, G. M. *Acta Crystallogr.* **2008**, A64, *112*.
7. Larson, A. C.; Von Dreele, R.B. *Los Alamos National Laboratory Report LAUR* 86-748 **1994.**
8. Coelho, A. A. TOPAS Academic 4.1.
9. Cerius2 Modeling EnVironment, Release 4.8; Accelrys Software Inc.: San Diego, **2005**.
10. de Vos Burchart, E. Ph.D. Thesis, Technical University of Delft, The Netherlands, **1992**; Table I, Chapter XII.